地震研究所彙報
Bull. Earthq. Res. Inst.
Univ. Tokyo
Vol. 75 (2000) pp. 1-13

Source Process of the Chi-Chi, Taiwan Earthquake of September 21, 1999 Inferred from Teleseismic Body Waves

Masayuki KIKUCHI, Yuji YAGI and Yoshiko YAMANAKA

Earthquake Research Institute, University of Tokyo, Tokyo, Japan

Abstract

Teleseismic body waves recorded at IRIS Global Seismographic Network are analyzed to investigate the source rupture process of the 1999 Chi-Chi earthquake. The azimuthal coverage of seismograph stations is good enough to resolve some details of heterogeneous moment-release. The source parameters obtained for the total source are: (strike, dip, slip)=(22°, 25°, 67°); the seismic moment=2.8×10^{20} [Nm] (Mw=7.6); the source duration=30 [s]; the fault area=75×40 [km^2]; the average dislocation=3.1 [m]; the stress drop=4.2 [MPa]. These values reveal typical features of large subduction zone earthquakes. A notable aspect of this earthquake lies in the highly heterogeneous manner of the moment-release. In the southern source area including the initial break, several small subevents were derived, which may be interpreted as ruptures of fault patches with a smaller length-scale. On the other hand, two large asperities with a length-scale of 20 km were obtained in the northern part of the source area: one in a shallow western part and the other in a deeper eastern part. The local stress drop on the former asperity was as high as 20 MPa and the fault slip exceeded 8 m, which is comparable to the ground displacement as inferred from both strong motion and GPS data. A high dip-angle nature of branch-faults in accretionary prism resulted in a considerable uplift of the hanging wall.

Key words: Taiwan earthquake, Source rupture process, Source parameter, Asperity, Waveform Inversion

1. Introduction

After midnight on September 21, 1999 (01: 47 local time), a devastating earthquake occurred near the town of Chi-Chi in central Taiwan. It left more than 2,400 people dead, 10,000 injured, and more than 6,000 collapsed houses. A destroyed dam with a vertical offset of about 10 m and waterfall due to the surface fault were broadcasted on TV news around the world.

The surface fault was traced along the known Chelungpu fault to about 80 km in a generally NS direction (Central Geological Survey of Taiwan, 1999). The fault offset varied from 1 to 8 m, and the largest offset appeared near the northern end of the surface fault.

According to the Central Weather Bureau (CWB) of Taiwan, the epicenter is 23.86°N, 120.81°E; the depth is 11 km; the local magnitude M_L based on the maximum acceleration is 7.3. On the other hand, according to Quick Epicenter Determinations

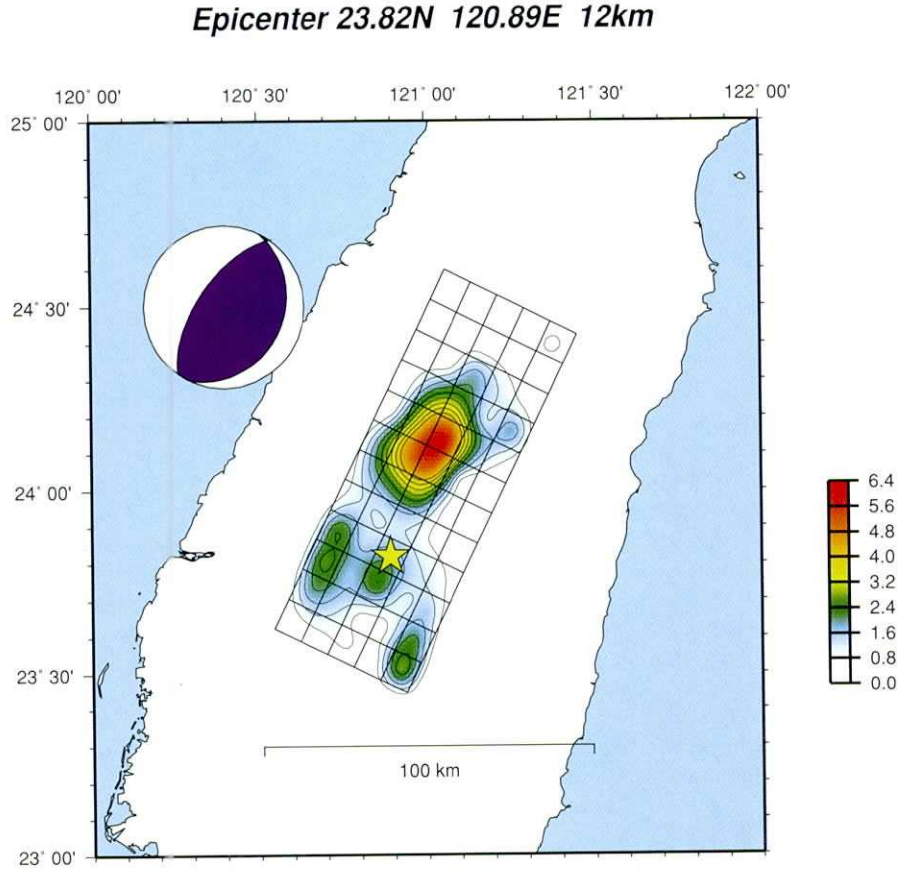

Fig. 1. Timely information on source rupture process of the 1999 Chi-Chi earthquake obtained by Yagi and Kikuchi (1999). This figure was posted on the web site the next day after the earthquake.

(QED) by NEIC, USA, the origin time is 17: 47: 18.4 UT, September 20, 1999; the epicenter is 23.728 N, 121.058 E; the depth is 5 km; the surface wave magnitude *Ms* is 7.7.

Soon after the earthquake, our institute, Earthquake Research Institute of the University of Tokyo, set up a special page on the web site: *http: //wwweic.eri.u-tokyo.ac.jp/topics/Taiwan/*, and tried to provide information about relevant researches and surveys on the Chi-Chi earthquake. A preliminary result of the source process was obtained on the following day from teleseismic data by Yagi and Kikuchi (1999), notifying that the major moment release occurred about 40 km north of the epicenter. It was posted at the web site as partly shown in Fig. 1. The number of accesses to this page exceeded 15,000 in the following two days.

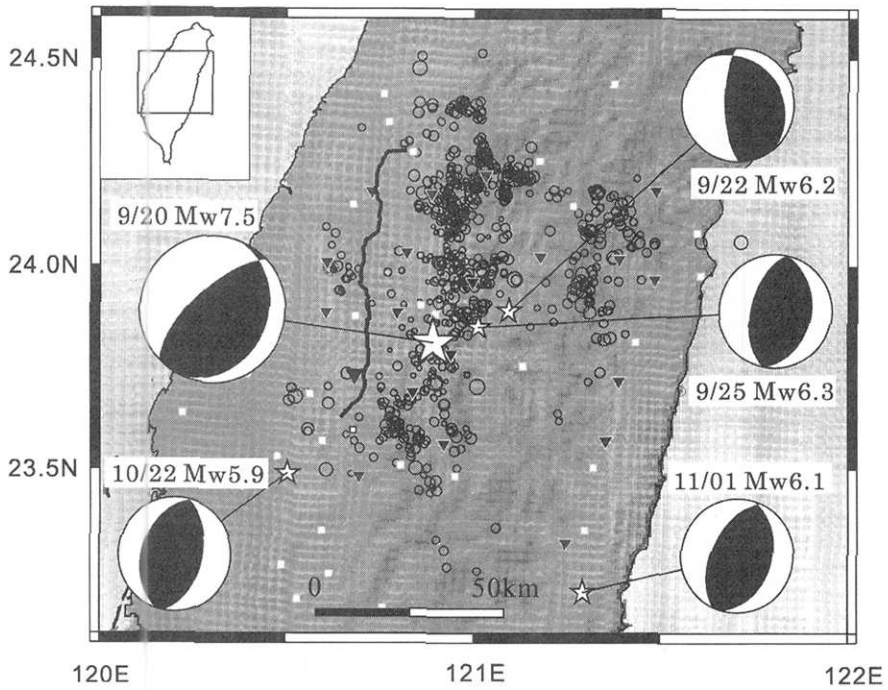

Fig. 2. Mechanism diagrams of main shock and the four largest aftershocks. The surface trace of the Chelungpu fault (Central Geological Survey of Taiwan, 1999) and the aftershock distribution (Hirata *et al.*, 2000) are also plotted.

In this paper we re-examine teleseismic data to extract information about source characteristics in collision-subduction regions, and to clarify the source effect on the spectral content of strong motion. Several major aftershocks are also analyzed using teleseismic data. All the earthquakes analyzed in this paper are shown in Fig. 2.

2. Teleseismic data analysis

Teleseismic broadband data were retrieved from Data Management Center of the Incorporated Research Institutions for Seismology (IRIS-DMC). We chose 17 stations and picked up body waves (vertical P and transverse S waves) for the analysis. The observation points are shown in Fig. 3 and the station parameters are given in Table 1. The azimuthal coverage is good enough to resolve some details of the moment-release distribution.

Using QED's epicenter and Jeffreys-Bullen's travel time table, the teleseismic data were windowed for two minutes starting 10 s before P-wave arrival or S-wave arrival. They were band-passed between 0.002–0.5 Hz, and converted to ground displacement with a sampling time of 1 s. Some examples of waveforms are shown in Fig. 3.

We employed an iterative deconvolution scheme developed by Kikuchi and

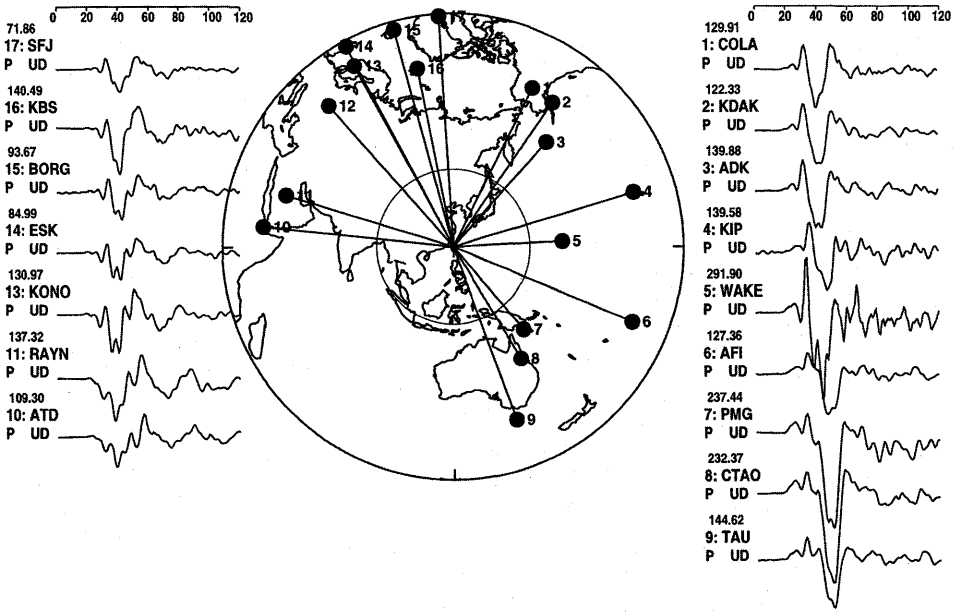

Fig. 3. IRIS broadband seismograph stations used in the present waveform inversion. The map is an equal distance projection. The inner and outer circles correspond to the epicentral distances of 30° and 90°, respectively.

Table 1. Station parameters

Station code	Azimuth [°]	Distance [°]	Phase
COLA	27.0	69.2	P-UD
KDAK	35.0	68.4	P-UD & SH
ADK	42.2	54.7	P-UD & SH
KIP	73.3	73.9	P-UD & SH
WAKE	86.9	42.7	P-UD
AFI	112.5	75.7	P-UD & SH
PMG	139.3	41.8	P-UD
CTAO	148.5	50.2	P-UD
TAU	159.8	70.7	P-UD & SH
ATD	276.0	74.6	P-UD & SH
RAYN	287.0	68.2	P-UD
KIEV	318.5	73.0	SH
KONO	331.4	79.8	P-UD & SH
ESK	331.9	87.9	P-UD & SH
BORG	334.8	87.0	P-UD & SH
KBS	348.9	70.3	P-UD & SH
SFJ	356.7	89.2	P-UD & SH

Table 2. Near-source structure used in the waveform inversion

V_P	V_S	ρ	D
4.00	2.14	2.35	1
5.60	3.23	2.70	5
6.50	3.75	2.85	30
7.80	4.40	3.30	-

T/Q_P=1.0[s] T/Q_S=4.0[s]

V_P, V_S = P-wave and S-wave velocities [km/s];
ρ = density [10^3 kg/m^3]; D = thickness [km]

Kanamori (1991), which is modified a little in this paper. First, with the approximation of a single point source, we determined the fault mechanism so that synthetic waveforms are fit best with the observed ones. For the synthetic waveforms we used a four-layer structure (three layers of crust and a semi-infinite mantle) in the source region as given in Table 2, referring to the structure by Rau and Wu (1995). At this step we assumed a long source duration of 25 s, which is comparable to the whole rupture time. The mechanism derived was a reverse fault given by (strike, dip, slip) =(22°, 25°, 70°) or (224°, 67°, 99°). We also made a grid search to determine the centroid source depth at 11 km. Moreover, using the time difference of P wave arrivals between observation and calculation based on Jeffreys-Bullen's table, we relocated the epicenter of the initial break at (23.82°N, 120.89°E), about 8 km east of the CWB's epicenter.

Next, fixing the focal mechanism, we constructed a grid scheme on the fault plane with six grid points along the fault strike with a spacing of 15 km and five grid points along the dip direction with a spacing of 10 km. Here, we considered a better spatial resolution along the dip direction than along the fault-strike. The iterative deconvolution was carried out to derive a series of subevents whose moment, onset-time, and location are unknown parameters. Inspecting the variance reduction with respect to the number of subevents, we derived 14 subevents, each having the source time function of an isosceles with a base width of 8 s. The procedure was performed for two possible fault planes: steep-dip and shallow-dip. It was found that the waveform match is slightly better in the case of a shallow-dip fault. Combining our result with aftershock distribution (Hirata *et al.*, 2000), we selected the eastward dipping plane as an actual fault plane.

In the final step of the inversion procedure, we relaxed the constraint of a fixed slip direction. To do this we took the strike-slip and dip-slip components as new model parameters, and determined their values by the linear least square method. We further modified the location and the onset-time of a few subevents within the nearest neighboring points so that moment release did not occur more than once at any grid point.

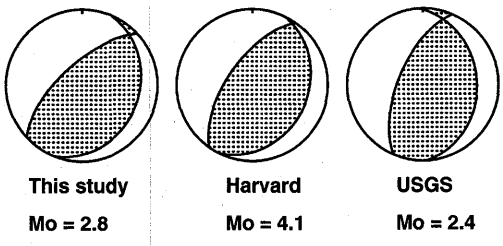

Fig. 4. Mechanism diagram of the total moment release. It is compared with the solutions obtained by Harvard University, and U.S. Geological Survey. The seismic moment is given in units of [10^{20} Nm].

3. Results

Our final solutions are shown in Figs. 4–6. The mechanism diagram for the total moment release is shown in Fig. 4. It is compared with other solutions obtained by Harvard University and U.S. Geological Survey. The number below the diagram indicates the seismic moment in units of 10^{20} Nm. Our solution coincides well with the other solutions. Fig. 5 (a) shows the moment-rate function, the area of which gives the total seismic moment: $Mo=2.8\times10^{20}$ Nm (Mw$=7.6$). The origin of the time-axis corresponds to the source origin time determined by USGS, 17: 47: 18.4 (UT). The centroid time by Harvard University, 17: 47: 38.2 (UT) is also shown. We neglected the moment release at a later stage after 40 s, which probably is a result of our inadequate modeling of the underground structure. In Fig. 5 (b), the spatial distribution of the subevents is represented by slip vectors, the length of which is proportional to the seismic moment. The number near the root of the slip vector indicates the rupture onset time [s]. The contour map shows the fault slip estimated from a moving average of the moment release among adjacent grid points. A map view of the fault slip is shown in Fig. 5 (c). A comparison between observed and resultant synthetic waveforms is shown in Fig. 6. Waveform match is satisfactorily good at all stations.

Let us first overview the properties of seismic source as a whole. The main source parameters are summarized in Table 3. The total rupture area is $S=75$ km (length)$\times$40 km (width). The source time duration is 30 s. The rupture front velocity is around 2.5 km/s as estimated from the onset time, 15 s, of the largest slip at 36 km distant from the initial break. The stress drop averaged over the entire fault plane is $\Delta\sigma=2.5Mo/S^{1.5}=4.2$ [MPa], which is comparable to or even slightly higher than the typical stress drop of subduction zone earthquakes (Kanamori and Anderson, 1975). The averaged dislocation is $D=Mo/\mu S=3.1$ m. All these source parameters reveal very standard features of a subduction zone earthquake. In contrast to the entire features, the details of the source process reveal much more specific and notable features of this earthquake as described below.

A small introductory rupture occurred preceding the main rupture by about 10 s.

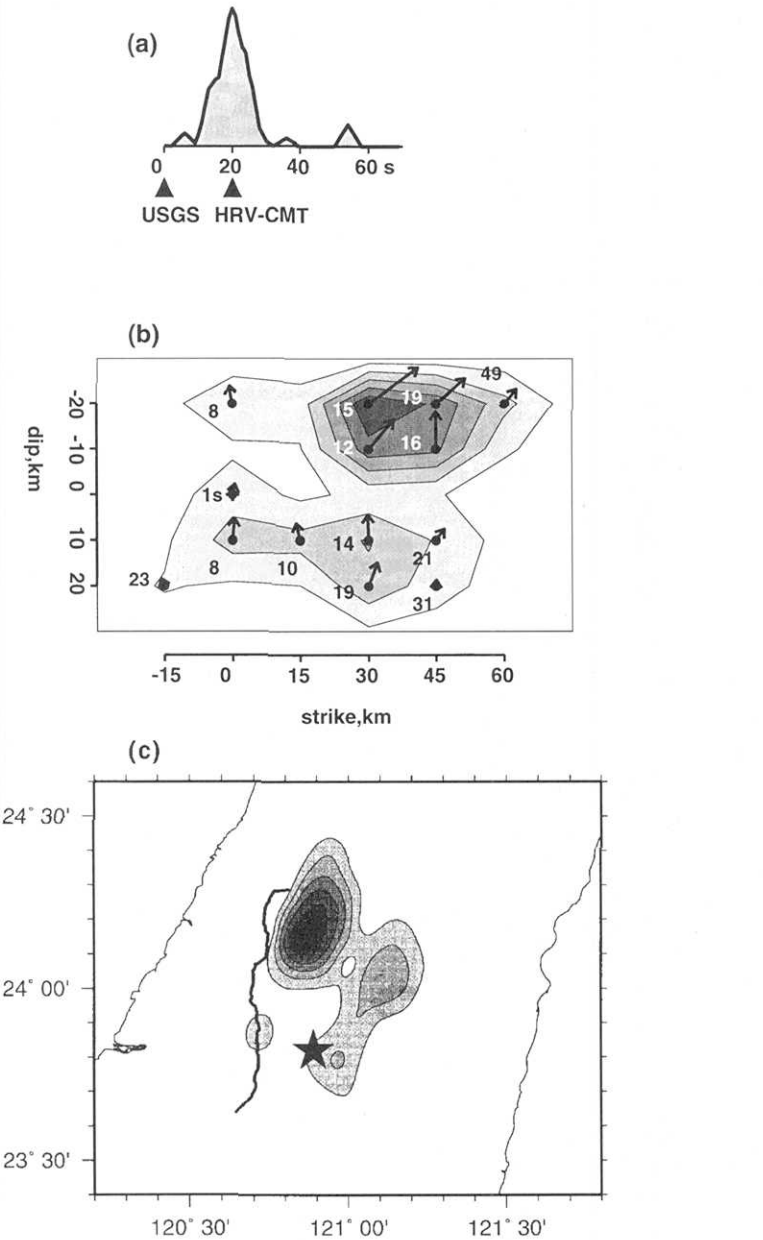

Fig. 5. (a) Moment-rate function. The origin of the time axis corresponds to the source origin time determined by U.S. Geological Survey. The centroid time determined by Harvard University is 20 sec later. (b) Spatial distribution of the moment release. The arrow indicates slip vector, the length of which is proportional to the seismic moment. The contour map was drawn by taking the moving average of the moment-release among adjacent grid points and converted into the fault slip. The contour interval is 2 m. (c) Map view of the fault slip derived.

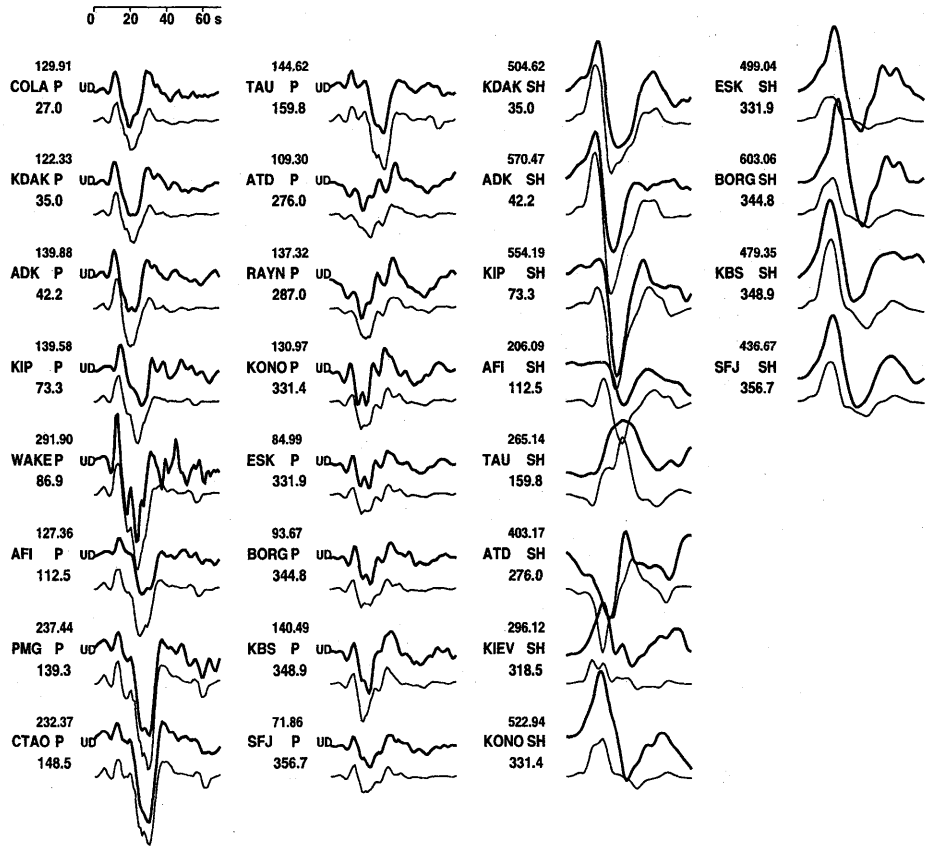

Fig. 6. Comparison of observed waveforms (upper trace) and synthetic waveforms (lower trace). The number above the station code indicates the peak-to-peak value of the observed displacement record [unit=micrometer], and the number below the station code is the source-to-station azimuth.

Initially, it expanded in the dip-direction (EW ward). The rupture then tended to propagate mainly to north, and there was a large slip motion. There are two major asperities: one (hereafter denoted as "asperity A") near ground surface and the other (hereafter denoted as "asperity B") in a deeper part. Both are located around 30 to 60 km north from the epicenter.

The seismic moment due to asperity A is $Mo_A = 1.5 \times 10^{20}$ Nm. Averaged over an area of $S_A = 30\,\text{km} \times 20\,\text{km}$, which may roughly outline the asperity, the fault slip is 8.6 m. The local stress drop is estimated as $\Delta\sigma_A = 2.5 Mo_A / S_A^{1.5} = 26$ [MPa]. It should be noted that the slip direction on this asperity is significantly different from that averaged in other source areas. The former is inclined to the northwest, while the latter is more westward. Such a variation of slip direction was also resolved in the teleseismic body wave analysis by Kao and Chen (2000).

For asperity B, the seismic moment $Mo_B = 0.65 \times 10^{20}$ Nm, and the fault slip

Table 3. Source parameters of the main shock

Origin time = 17:47:19, Sep. 20, UT (01:47:19, Sep. 21, local time)
Epicenter = 28.32° N, 120.89° E

Total	
(strike, dip, slip)	= (22° , 25° , 67°)
Seismic moment	$Mo = 2.8 \times 10^{20}$ [Nm]
	(Mw= 7.6)
Source duration	= 30 [s]
Depth extent	11±8 [km]
Fault area	$S = 75 \times 40$ [km^2]
Average dislocation	$D = Mo/\mu S$ = 3.1 [m]
Stress drop	$\Delta\sigma = 2.5\, Mo/S^{1.5}$ = 4.2 [MPa]

Asperity	A	B
Slip-angle[°]	52	76
Seismic moment [10^{20} Nm]	1.5	0.65
Source duration [s]	15	14
Fault area [km^2]	30×20	30×20
Average dislocation [m]	8.6	3.6
Stress drop [MPa]	26	11

averaged over an area of S_B=30 km×20 km is 3.6 m. The local stress drop is $\Delta\sigma_B$= 11 [MPa]. These two asperities seem to correlate with the distribution of aftershock clusters (Hirata *et al.*, 2000). Kao and Chen (2000) examined the mechanism of major aftershocks and obtained the normal faults on the western side beyond this asperity.

In addition to these asperities, several smaller subevents are found in the southern part of the fault plane. Three are located within 18 km from the initial break. The total seismic moment for the subevent cluster is 4.7×10^{19} Nm, and the average fault slip is 3.5 m. Considering the isolation of subevents in time and space, we interpret these subevents as ruptures of individual fault patches with a shorter length-scale, although we cannot resolve the details from a teleseismic analysis alone. Such a small-scale heterogeneity would affect the spectral contents of a generated strong motion.

4. Discussion

Large offset

All the geological and geophysical observations such as surface fault, GPS data, and strong-motion data indicate a ground displacement as large as 8 m near the

northern end of the hanging wall. Our result also shows that a large fault slip exceeding 8 m occurred co-seismically near the end of the fault plane. Thus, as a first order approximation, the large displacement observed on the hanging wall is interpreted simply as a manifestation of the fault slip on the asperity. In this sense a thick soft layer covering the seismogenic zone did not amplify or attenuate the ground displacement.

Not a slow earthquake

In spite of a large fault offset there was little damage except in the narrow band just across the fault trace (Seno *et al.*, 2000). This fact leads us to suspect that the speed of fault motion was very slow. The slowness of the source process can be measured from the value of Mo/T^3, where Mo is seismic moment and T the source duration. For ordinary shallow earthquakes, empirical relations have been proposed as follows (Furumoto and Nakanishi, 1983; Ekström and Engdahl, 1989):

$$Mo/T^3 = 0.25 - 1 \times 10^{16} \ [\mathrm{Nm/s^3}]$$

For slow earthquakes, the value of Mo/T^3 must be much smaller than the above value. In fact, the 1992 Nicaragua earthquake, which is considered to be a slow earthquake (Kanamori and Kikuchi, 1993), gives $Mo/T^3 = 3 \times 10^{14}\,\mathrm{Nm/s^3}$. For the Chi-Chi earthquake, we obtained $Mo/T^3 = 1 \times 10^{16}\,\mathrm{Nm/s^3}$. This value lies within the range of ordinary earthquakes. Moreover, the ground velocity observed at the northern end of surface fault was as large as 3 m/s, which is the largest ground velocity ever recorded in the world. Thus the Chi-Chi earthquake is not considered to be a slow earthquake.

Tsunami earthquake on land?

Seno *et al.* (2000) proposed an interesting idea that this earthquake can be regarded as a tsunami earthquake on land. They thought that a large uplift of the basement was enhanced by a ductile deformation of trench wedge sediment, which was pushed by accretionary prism. The essential point of their model is that even a very low dip angle of the seismic faulting near the trench axis could produce a large vertical motion of the basement. We agree that the Chi-Chi earthquake possesses a property of a tsunami earthquake in the sense that if the source area were under the sea, it would cause larger tsunami than expected from the seismic magnitude. In the present case, however, the seismic faulting alone can produce a large uplift of the basement due to a relatively high dip-angle. The Chelungpu fault is a branch fault in the accretionary prism, whose dip angle is usually higher than that of slab interface earthquakes. It would be as high as 30° or more near the ground surface. Thus the Chi-Chi earthquake possesses a property of a tsunami earthquake as proposed by Fukao (1979).

Spectral content of strong ground motion

More than 400 digital accelerometers were operated at the earthquake occurrence and recorded strong motions at various sites around the source area. It is very notable that the strong motion data was provided to worldwide researchers via

Table 4 Source parameters of the largest aftershocks

Origin Time	Epicenter	Depth	(strike, dip, slip)	*Mo*	*T*	Mo/T^3
9/20 17:47:19	23.82N 120.89E	11	(22, 25, 67)	2.8	30	1.0
9/22 00:14:40	23.90N 121.09E	27	(320, 24, 54)	.024	6	1.1
9/25 23:52:51	23.86N 121.01E	11	(11, 36, 89)	.041	10	.40
10/22 02:18:59	23.50N 120.50E	16	(12, 49, 86)	.0077	4	1.2
11/01 17:53:00	23.21N 121.29E	30	(16, 38, 83)	.021	6	.97

Origin-time [UT]; Epicenter [°]; Depth[km]; (strike, dip, slip) [°]
Mo: Seismic-moment[10^{20} Nm]; *T*: Source duration [s]; Mo/T^3: [10^{16} Nm/s^3]

CD-rom. The data indicate a general tendency that the peak of ground acceleration is larger and the peak frequency is higher in the southern area, while ground displacement and velocity are larger in the northern area. Such a tendency seems to be consistent with our interpretation of the different asperity sizes in the northern part and the southern part of the fault plane. Suppose a shear cracking occurs instantaneously over a circular plane with diameter d, then the predominant period of slip motion is roughly given by $d/2\beta$where β is the shear wave velocity. Asperities of the present earthquake have a length-scale of $d\sim20$ km, so that the predominant period is about 3 s. In comparison, the 1995 Kobe earthquake was accompanied by asperities with a length scale of $d=5\sim10$ km (e.g., Yoshida *et al.*, 1996), resulting in a predominant period of about 1 s. The spectral content of strong ground motion may affect which houses are seriously damaged. Sakai *et al.* (2000) pointed out that the spectral amplitude of about 1 Hz is critical to the collapse of low-rise buildings.

High local stress drop

In an attempt to examine the stress level around the source region, we chose several large aftershocks to calculate the value of Mo/T^3, which is a measure of the stress drop. The source parameters derived from teleseismic data are given in Table 4. The mechanism diagram is shown in Fig. 2. All these aftershocks are reverse faults similar to the main shock, but the source depth varies beyond the source area of the main shock. As shown in Table 4, the derived value of Mo/T^3 for the aftershocks is nearly the same as the value for the main shock. This suggests that the stress level surrounding the source region was not very heterogeneous.

On the other hand, the local stress drop, 26 MPa, on the largest asperity is particularly high at about six times as high as the average stress drop, 4.2 MPa. When viewing a large fault slip combined with the high stress drop, we may think that some microscopic process such as the melting or fluid pressurization might occur around the slip plane and reduce the final stress to a level much less than ordinary dynamic friction of a solid interface. (Kanamori *et al.*, 1998). Thus it would be very challenging to confirm this by direct observation through a borehole in the asperity region.

Acknowledgement

We would like to thank Hitoshi Kawakatsu and Satoshi Ide for their critical review. This research was partially supported by the Grant-in-Aid for Scientific Research No. 11694056 from the Ministry of Education, Japan.

References

Central Geological Survey (Taiwan), 1999, Map of surface ruptures, posted at *http: //www. moeacgs.gov.tw/921/envi921/*

EKSTRÖM, G. and E.R. ENGDAHL, 1989, Earthquake source parameters and stress distribution in the Adak Island region of the Central Aleutian Islands, Alaska, *J. Geophys. Res.*, **94**, 15499–15519.

FUKAO, Y., 1979. Tsunami earthquakes and subduction processes near deep-sea trenches, *J. Geophys. Res.*, **84**, 2303–2314.

FURUMOTO, M. and I. NAKANISHI, 1983, Source times and scaling relations of large earthquakes, *J. Geophys. Res.*, **88**, 2191–2198.

HIRATA, N., S. SAKAI, Z.-S. LIAW, Y.-B. TSAI and S.-B. YU, 2000, Aftershock observation of the 1999 Chi-Chi, Taiwan, earthquake, *Bull. Earthq. Res. Inst.*, this issue.

KANAMORI, H. and D.L. ANDERSON, 1975, Theoretical basis of some empirical relations in seismology, *Bull. Seism. Soc. Am.*, **65**, 1073–1095.

KANAMORI, H., D.L. ANDERSON and T.H. HEATON, 1998, Frictional melting during the rupture of the 1994 Bolivian earthquake, *Science,* **279**, 839–842.

KANAMORI, H. and M. KIKUCHI, 1993, The 1992 Nicaragua earthquake: a slow tsunami earthquake associated with subducted sediments, *Nature,* **361**, 714–716, 1993.

KAO, H. and W.-P. CHEN, 2000, The Chi-Chi earthquake sequence: active, out-of-sequence thrust faulting in Taiwan, *Science,* **288**, 2346–2349.

KIKUCHI, M. and H. KANAMORI, 1991, Inversion of complex body waves-III, *Bull. Seismol. Soc. Am.*, **81**, 2335–2350.

RAU, R. and F.T. WU, 1995, Tomographic imaging of lithospheric structure under Taiwan, *Earth Planet. Sci., Lett.*, **133**, 517–532.

SAKAI, Y., K. KOKETSU, S. YOSHIOKA and T. KABEYASAWA, 2000, Damage to buildings by the 1999 Taiwan Chi-Chi earthquake and response analyses using recorded strong ground motions, *Bull. Earthq. Res. Inst.*, this issue.

SENO, T., K. OTSUKI and C.-N. YANG, 2000, The Sept. 20, 1999 Chichi earthquake in Taiwan: a subduction zone earthquake on land, *Bull. Earthq. Res. Inst.*, this issue.

YAGI, Y. and M. KIKUCHI, 1999, Spatiotemporal distribution of the source rupture process for the Taiwan earthquake (Ms 7.6), posted at *http: //wwweic.eri.u-tokyo.ac.jp/yuji/taiwan/*

YOSHIDA, S., K. KOKETSU, B. SHIBAZAKI, T. SAGIYA, T. KATO and Y. YOSHIDA, 1996, Joint inversion of near- and far-field waveforms and geodetic data for the rupture process of the 1995 Kobe earthquake, *J. Phys. Earth,* **44**, 437–454, 1996.

(Received April 27, 2000)
(Accepted June 21, 2000)

遠地実体波解析による1999年9月21日台湾中部集集地震の震源過程

菊地正幸・八木勇治・山中佳子

東京大学地震研究所地震予知情報センター

グローバル広帯域地震計観測網の遠地実体波記録を用いて，1999年台湾中部地震の震源過程を調べた．観測点の方位分布は良好であり，大まかな不均一断層すべり分布が抽出された．主な震源パラメーターは次の通り．断層メカニズムは東傾斜面の衝上断層で（走向，傾斜，すべり角）＝（22°，25°，67°）；地震モーメント＝2.8×10^{20} Nm（Mw＝7.6）；破壊継続時間＝30 s; 断層面積＝75×40 km^2; 平均すべり量＝3.1 m; 平均応力降下＝4.2 MPa．これらの震源パラメーターは沈み込み帯におけるプレート境界大地震の標準的な値である．しかし今回の地震の際だった特徴は断層すべりの不均一性にある．まず，破壊開始点を含む断層面の南側の領域では，比較的小さい断層パッチが次々と動いたことが示唆された．一方，断層面の北側では，さしわたし約20 kmの2つの大きなアスペリティ（大きい地震時すべりを起こす領域）が動いたとの結果が得られた．1つは西側の浅いところ，もう1つは東側の深めに位置する．浅い方のアスペリティでは応力降下が26 MPa，すべり量は8 m強である．このすべり量は，GPSデータや強震記録から推定された断層上盤側の最大変位量と同程度である．付加帯内部への分岐断層の特徴として断層面の傾斜が比較的高角であるため，プレート上面の地震の場合と比べて，上盤側の隆起量が大きい．仮に震源が海底にあったとすると，地震の規模から経験的に予測されるより大きい津波を引き起こしたはずである．